Micropatterned lead zirconium titanate thin films

J.S. Vartuli[a)]
Department of Chemical Engineering, Princeton University, Princeton, New Jersey 08544-5263
M. Özenbaş
Department of Metallurgical and Materials Engineering, Middle East Technical University, Ankara 06531, Turkey
C-M. Chun,[b)] M. Trau,[c)] and I.A. Aksay
Department of Chemical Engineering, Princeton University, Princeton, New Jersey 08544-5263

(Received 20 February 2003; accepted 26 February 2003)

Micropatterning of $Pb(Zr_{0.52}Ti_{0.48})O_3$ (PZT) thin films with line features as small as 350 nm was demonstrated through capillary molding of organometallic solutions within the continuous channels of an elastomeric mold. Despite the large stresses that develop during the evaporation of the solvent, pyrolysis of the organics, and the densification and crystallization of the inorganic gel, the patterned crystalline PZT films were crack-free and mechanically robust. Flawless regions as large as 1 cm^2 were obtained. The cross-sectional shape of the patterned PZT lines was trapezoidlike. Single perovskite PZT grains that formed during annealing at 600–700 °C completely filled the cross-sectional area of the patterned lines. Lead acetate, zirconium propoxide, and titanium isopropoxide were used as the starting materials. Substrates used included silver tape, stainless steel plate, silicon wafer, and platinum-coated silicon wafer.

I. INTRODUCTION

Ferroelectric thin films are playing an increasingly important role in integrated electronic devices as capacitors, piezoelectric materials (transducers), pyroelectric detectors, electro-optic materials, thermistors, and dielectrics.[1] Ferroelectric thin films with micron-scale patterns are also receiving increasing interest for use in microelectromechanical systems (MEMS).[2] MEMS combine the traditional silicon-based integrated-circuit electronics with micromechanical sensing and actuating components. The term MEMS has become synonymous with many types of microfabricated devices such as accelerometers, infrared detectors, flow meters, pumps, motors, and mechanical components.[3] These devices have lateral dimensions in the range of 0.1 μm to 1 mm. Commercial applications for MEMS already span biomedical (e.g., blood-pressure sensors),[4] manufacturing (e.g., microflow controllers),[5] information processing (e.g., displays),[6] and automotive (e.g., accelerometers)[7] industries. More applications are projected in consumer electronics, manufacturing control, communications, and aerospace.[8–10] The superior piezoelectric and pyroelectric properties of inorganic ferroelectric materials make them ideal for use in microactuators and microsensors.

The ability to create submicron-sized patterned ceramic structures is highly desirable in the fabrication of microelectronics, optical devices, and micromechanics. The growing interest in fabricating miniaturized ceramic structures has resulted in a number of new fabrication methods[11–19] based on soft lithography techniques pioneered by Whitesides and colleagues.[20] In soft lithography, an elastomeric [e.g., polydimethylsiloxane (PDMS)] mold with features as small as 30 nm is used to generate patterns on flat or curved surfaces.[20] So far, three different modes of soft lithography have been used to process patterned ceramics with micron-sized features. All three methods are quick and inexpensive procedures that permit the creation of nanoscale features without the stringent requirements of a clean room.

The first method utilizes microcontact printing (μCP)[21] to transfer self-assembled surfactant monolayers [SAMs; e.g., octadecyltrichlorosilane (OTS)] from an elastomeric mold to a substrate.[11–13,16] A sol-gel precursor is then spin cast on top of the patterned SAM to produce a continuous film. After pyrolysis of the organics, the portions of the sol-gel film on the OTS covered surface severely crack and show poor adhesion.[11] Mild mechanical abrasion with a damp cotton felt or washing with isopropanol is used to remove the poorly adhered

[a)]Present address: General Electric, Corporate Research & Development, Schnectady, New York 12301.
[b)]Present address: Exxon-Mobil Research & Engineering Company, Annandale, New Jersey 08801.
[c)]Present address: Department of Chemistry, University of Queensland, St. Lucia, QLD4067, Australia.

regions. Once the flakes are removed, the remaining patterned film undergoes its final heat treatment to convert the precursor to the desired oxide. Patterned films of $LiNbO_3$ and (Pb,La)TiO_3 on Si, Al, Pt, and ITO with linewidths of 4–300 μm,[11] Ta_2O_5 on Pt/Si with features as small as 4 μm,[11] and Pt/Pb($Zr_{0.52}Ti_{0.48}O_3$/Pt on TiN/SiO_2/Si with a linewidth of 200 μm have been reported.[13]

Channel stamping developed by Lange and colleagues is the second version of soft-lithography for the micropatterning of ceramics.[17,18] In this method, the channels of a PDMS stamp are first filled with an organometallic precursor solution by spin coating. After solvent evaporation, the solidified precursor within the channels is transferred to a substrate by stamping. This method has been used to grow patterned epitaxial $SrBi_2Ta_2O_9$ of 50 μm wide lines on a $SrTiO_3$ substrate.[17]

The third method is based on micromolding in capillaries (MIMIC) of a patterned PDMS mold when it is placed on a substrate.[22–24] MIMIC is a single-step process and has been shown to produce features as fine as 500 nm.[14,19] Thus, in applications requiring submicron scale features, MIMIC provides a clear advantage over the μCP and channel-stamping techniques. Further, since the capillaries can be used as microreactors, this method has also been used to impose a hierarchy of structures on thin solid films by combining surfactant self-assembly for templating nanoscale channels with silica.[14,15] MIMIC has recently been used to generate patterned microstructures of ZrO_2 and SnO_2 from their polymeric precursors.[19]

The specific focus of the work reported here is on micropatterning of crystalline Pb($Zr_{0.52}Ti_{0.48}$)O_3 (PZT) thin films by the MIMIC technique. The unique geometry provides an opportunity to study the confined one-dimensional grain growth of the perovskite phase within a fluorite (pyrochlore) matrix. Previous studies have characterized the growth of perovskite phase within a fluorite matrix of a continuous thin film;[25–28] however, no studies have yet been performed on one-dimensionally-confined systems.

II. EXPERIMENTAL

A. Solution preparation

The preparation of the liquid inorganic precursor solutions was carried out by a method similar to that reported by Yi *et al.*[29] Lead (II) acetate trihydrate, zirconium (IV) propoxide, and titanium (IV) isopropoxide (all from Aldrich, Milwaukee, WI) were used as the starting materials. Precursor solution was prepared by first dissolving lead acetate trihydrate in glacial acetic acid with a 2:1 mass ratio and then boiling off water at 105 °C for <5 min. This solution was then mixed with appropriate amounts of zirconium propoxide and titanium isopropoxide to produce Pb($Zr_{0.52}Ti_{0.48}$)O_3. The solution was agitated by mixing in an ultrasonic bath to dissolve any residual condensed solid. Ethylene glycol was then added in the proportion of 1 ml to 10 g of lead acetate in solution to prevent cracking and to improve the surface smoothness of continuous films; but this step was not necessary for the patterned films. The initial reaction had to be complete before the glycol was added since residual titanium isopropoxide and zirconium propoxide alcolyze with ethylene glycol to form a condensed solid. The solution was diluted with distilled water or *n*-propanol to adjust the viscosity and surface tension of the solution to improve the surface coverage of the liquid within the mold.

B. Micromolding in capillaries

The general procedure for MIMIC, shown schematically in Fig. 1, has been described elsewhere.[20,22–24] A master is first produced by patterning silicon, either by photolithographic or non-photolithographic techniques to produce relief features. This master is then used to fabricate the elastomeric PDMS mold from Sylgard 184 (DOW Corning, Midland, MI). The PDMS mold is placed down on a substrate and the recessed microchannels are used to wick a liquid precursor [Fig. 1(a)]. In our case, the PZT precursor was added drop wise along the sides of the mold. Capillary forces spontaneously pull

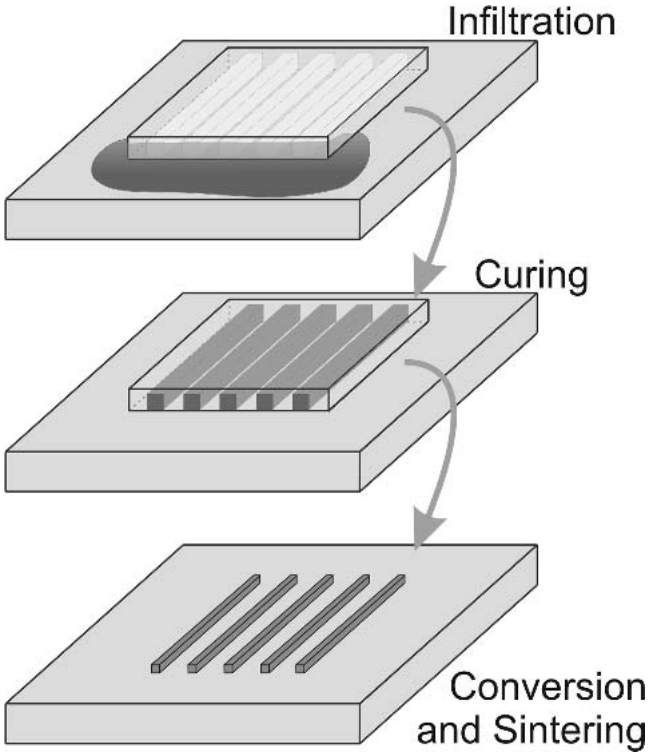

FIG. 1. Schematic diagram of the MIMIC process used in this study.

the sol-gel solution into the micron-sized channels. Reduction in the viscosity of the solution increased the surface area coverage of the patterned material.

The precursor solution was allowed to dry in air at room temperature with the PDMS mold in place. Once the gel was sufficiently dry, the PDMS mold was peeled off from the supporting substrate. The dried organometallic remained firmly bound to the substrate and did not attach itself to the PDMS mold. The low surface energy of the PDMS mold ($\gamma_{PDMS\text{-}air} = 21.6$ dyn cm^{-1}) and the lack of any reaction with the PZT precursor helped to keep the adhesion between the PZT gel and the PDMS mold low.[22]

Micromolding was performed on a variety of substrates, including (100) oriented silicon wafers, 100 nm thick Pt-coated (100) silicon wafers, stainless steel plates, and silver and platinum foils. All substrates were degreased and cleaned prior to patterning. Experiments on all substrates displayed patterns with similar appearance and integrity.

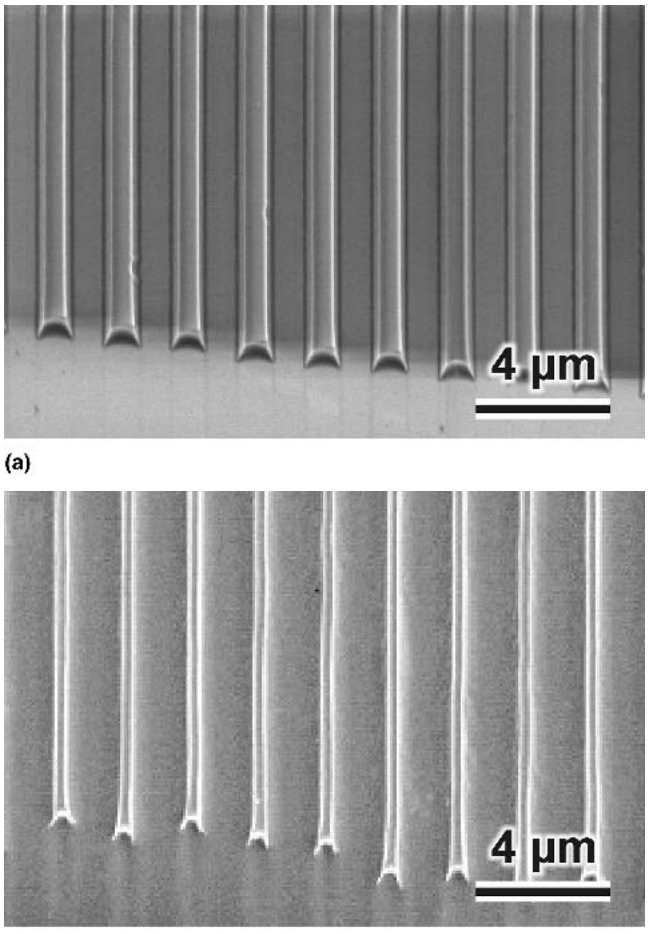

FIG. 2. SEM images of line patterns grown on a silicon substrate within 1-μm-wide channels of a PDMS mold (a) after drying at room temperature and (b) after annealing at 600 °C for 3 h.

C. Heat treatment

The final step in the processing was the conversion of the gel to the perovskite phase by heat treating the films at a suitable temperature to ensure full crystallization. Heat treatments were done in electric resistance furnaces by heating the samples to the annealing temperature at a rate of 10 °C/min. Annealings were done between 600 and 700 °C for 3 to 5 h.

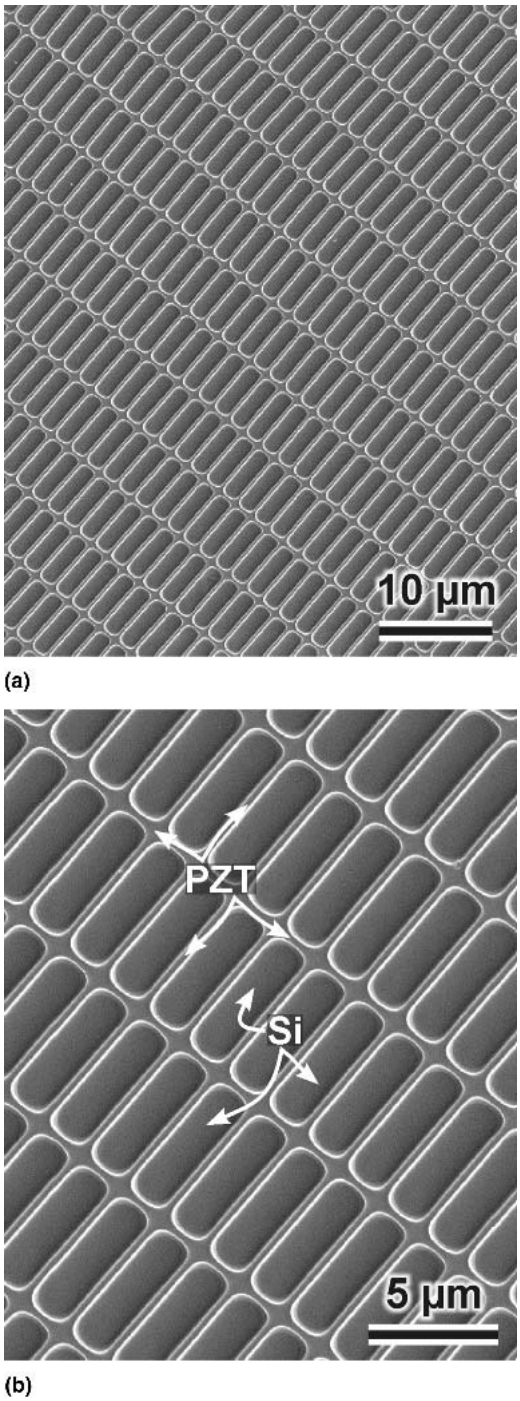

FIG. 3. Low and high magnification SEM images of a micropatterned PZT net on a silicon substrate after annealing at 600 °C for 3 h.

D. Characterization

The overall appearance of the films was examined by a Philips XL30 field emission gun scanning electron microscope (FEG-SEM) (FEI Company, Salem, MA) and a Jeol SEM-6400 (JEOL, Peabody, MA). The samples for the FEG-SEM study were coated with carbon and examined at 2.0 keV. Qualitative energy dispersive spectroscopy (EDS) for chemical analysis was performed with a Tracor-Northern detector and associated software on the Jeol SEM-6400 (JEOL, Peabody, MA). A Philips XRG-3100 (FEI Company, Salem, MA) powder x-ray diffraction analyzer (XRD) was used to study the crystallization of the gels. Powder samples for the XRD were obtained by scraping the patterned substrates. Further investigation by transmission electron microscopy (TEM) was performed with a Philips CM200 FEG-TEM (FEI Company, Salem, MA) operated at 200 keV. The plane-view and the cross-sectional samples were prepared by standard techniques and the identification of the crystalline phases was done in selected-area electron diffraction (SAED) mode.

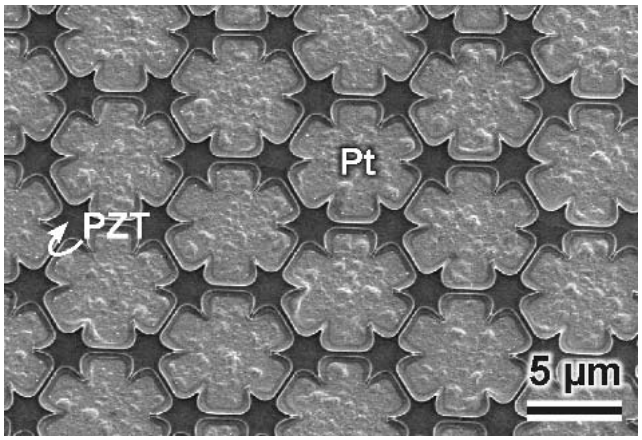

FIG. 4. SEM image of micropatterned PZT on platinum coated silicon wafer after annealing at 600 °C for 3 h.

III. RESULTS AND DISCUSSION

A. Morphological changes of micropatterned lines during heat treatment

SEM images of the micropatterned lines produced on a Si wafer with 1-μm-wide channels of a PDMS mold are shown in Fig. 2(a) after mold release and Fig. 2(b) after annealing at 600 °C for 3 h. More complicated PZT micropatterns are shown in the SEM images of Figs. 3 and 4. In all cases, defect-free regions as large as 1 × 1 cm were obtained. Beh *et al.*[19] also illustrated that micropatterned ZrO_2 and SnO_2 thin films as large as 1 cm^2 could be produced by the MIMIC method. While it was easy to obtain crack-free patterned films on all substrates, adhesion seemed to be weaker on stainless steel plates compared to the other substrates.

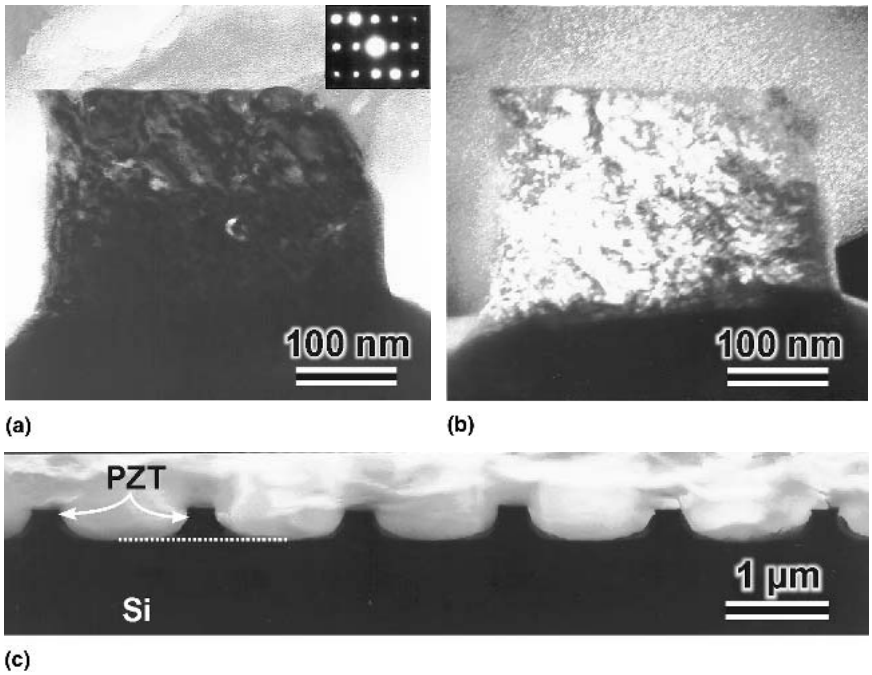

FIG. 5. Cross-sectional TEM images of micropatterned PZT lines on a silicon substrate: (a) bright-field image of one PZT line, (b) dark field image of the same line, and (c) bright-field image of an array of lines at low magnification. The insert shows the electron diffraction pattern for the perovskite phase at the zone axis of [011]. The dotted line in (c) corresponds to the interface between PZT lines and the Si substrate. The TEM sample was prepared by ion milling of a cross-sectioned sample that was annealed at 600 °C for 3 h.

A comparison of Figs. 2(a) and 2(b) indicates a considerable shrinkage in the line width after the annealing step. The TEM images (Fig. 5) of the cross sections of the annealed PZT lines on Si show that the lines are trapezoidlike. The top surface of the lines is about 350 nm wide and the bottom is about 400 nm wide. The sides are sloped with visible concavity. Since prior to drying and heat treatment the cross section of the lines was rectangular, measuring 1 μm high and 1 μm wide for the pattern shown in Fig. 2, this observation indicates nonuniform shrinkage during the heat treatment across the lines. The length of the top portion is more than 12% smaller than the bottom length indicating that the lines are pinned to the substrate and the shrinkage at the Si/film interface is more constrained. Average volumetric shrinkage of the PZT lines after the heat treatment on Si, Pt/Si, and stainless steel substrates was 20%, 21%, and 26%, respectively. These values are comparable to those reported by Beh *et al.*[19] on micropatterned ZrO_2 and SnO_2 thin films. As discussed below, this lateral shrinkage appears to be essential for the defect-free fabrication of patterned films when the film thickness is larger than 0.1 μm.

B. Crystallization of micropatterned lines

Micropatterned films were initially amorphous, and annealing was needed to convert them to a ferroelectric form to obtain the desirable ferroelectric properties. Prior studies have shown that during heat treatment an intermediate pyrochlore phase is the first crystal that forms before the nucleation and growth of the desired perovskite structure at a higher temperature.[25–28] For the film compositions used in this study, a Zr/Ti molar ratio of 52/48, the perovskite phase after annealing was expected to be tetragonal.[26,27] Cross-sectional bright- and dark-field TEM images (Fig. 5) of the PZT lines on a silicon substrate illustrate the formation of the perovskite PZT phase after annealing at 600 °C for 3 h. The SAED shows a spot pattern at the zone axis of [011], emphasizing the single crystallinity of the perovskite PZT in the entire cross section. By using SAED, we also detected the presence of a fluorite PZT (pyrochlore) as the minority phase.

Previous studies on continuous thin films showed that the perovskite phase nucleates and grows through a nanocrystalline pyrochlore matrix towards the surface of the film, forming a columnar nanostructure at or above 600 °C.[30–33] Our TEM observations agreed with these findings. The perovskite phase nucleated at the film-substrate interface (Fig. 6) and rapidly filled the entire cross-section of the pattern line yielding the single crystalline cross-sections illustrated in Fig. 5. Once the perovskite phase completely fills the cross section of the line, further growth of the grain now has to be on a one-dimensional path along the line. Although we have not performed a detailed study along the lines, a bamboolike line pattern is expected to result.

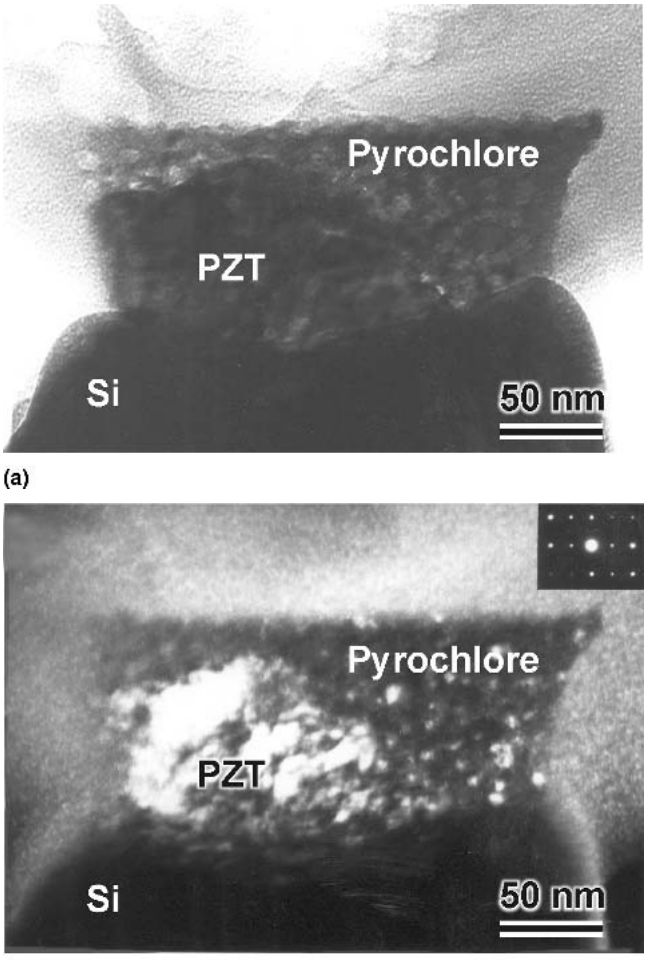

FIG. 6. TEM images of 1 μm lines of PZT on silicon heat treated at 600 °C for 2 h. (a) Bright field and (b) Dark field cross-sectional images illustrate the formation of perovskite rosette in pyrochlore matrix at the Si/film interface. The insert shows the electron diffraction pattern for the perovskite phase at the zone axis of [011].

XRD studies of the powders scraped from the patterned films supported the results of the TEM work and provided additional data on the role of annealing temperature and time. As shown in Fig. 7, the perovskite phase is clearly the majority phase after a 3 h annealing at 600 °C. Pyrochlore is detected as the minority phase. After a 5-h anneal, however, the pyrochlore phase is barely detectable. Similarly, when the heat-treatment temperature is increased to 650 and 700 °C (Fig. 8), the pyrochlore phase is again barely detectable. At higher annealing temperatures, all the XRD peaks shift slightly toward higher angles. This phenomenon is related to changes in the composition and defect structure of the film.[29]

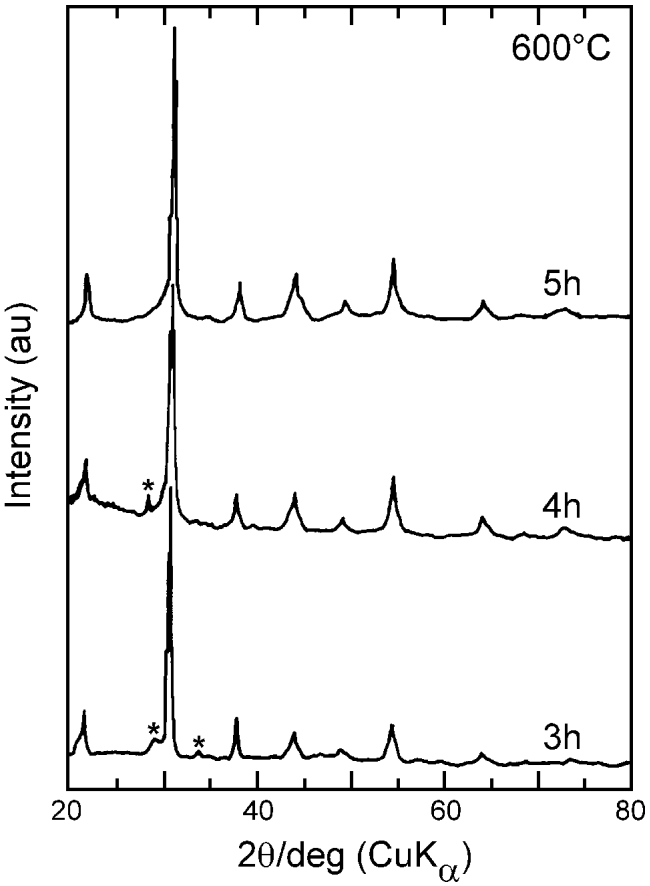

FIG. 7. XRD spectra of the patterned PZT films as a function of the annealing period at 600 °C. Pyrochlore phase is indicated by an asterisk on the spectra. All other peaks correspond to the perovskite phase.

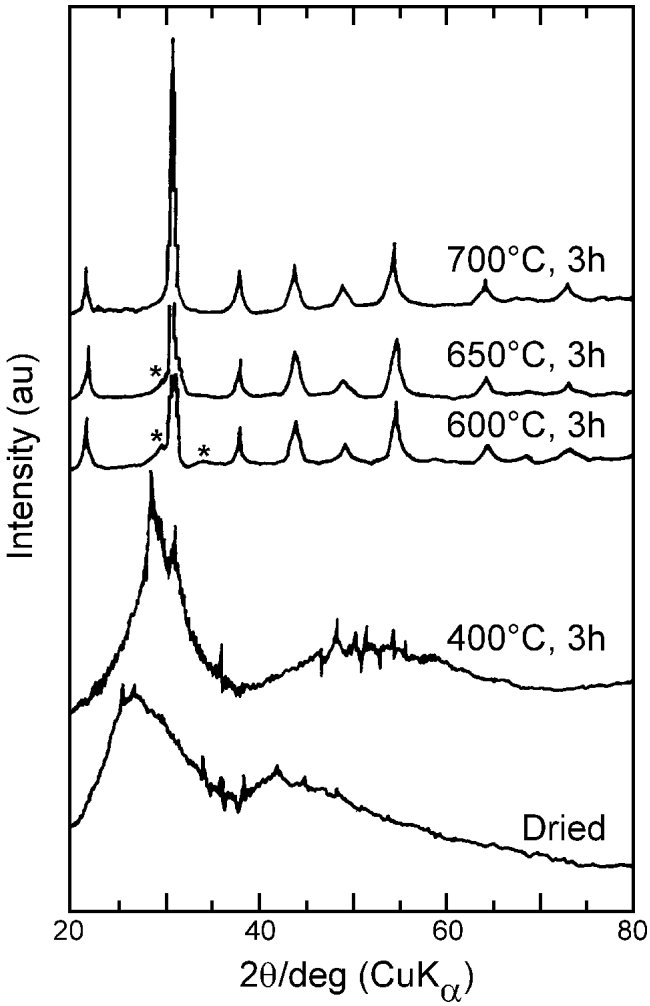

FIG. 8. XRD spectra of the patterned PZT films as a function of the annealing temperature. Pyrochlore phase is indicated by an asterisk on the spectra. All other peaks correspond to the perovskite phase.

Although heat treatments above 600 °C or longer times were beneficial in the elimination of the pyrochlore phase, films then developed rough surfaces and in some cases detached from the substrate. The EDS analysis of the patterned films (Fig. 9) also showed that the required composition is retained after the 600 °C heat treatment. Thus, the optimum heat treatment procedure was decided to be 600 °C for 3 h.

C. Robustness of patterned films

Few cracks or defects were observed in the patterned films of 1 μm in thickness when the films were heat treated at 600 °C (Figs. 2–4). In contrast, continuous PZT thin films of similar thicknesses fabricated under similar conditions showed cracks due to the stresses developed during drying and heat treatment. In all micropatterned films, the PZT–substrate interface was intact, and there was no evidence that the patterned film slid across the surface of the substrate. This indicates that the adhesion forces were strong enough to counteract the stresses developed during drying and heat treatment.

Although the adhesion forces are expected to be the same for the patterned and the continuous films, the robustness of the patterned films is related to the relaxation of the stresses during lateral shrinkage. With continuous sol-gel processed thin films, lateral shrinkage is not allowed and if the thickness of the gel exceeds 100 nm, the film is likely to crack due to the strain energy stored in the film.[34] The calculations based on Griffith's criteria account for a balance between strain energy stored in the film and the energy released from cracking.[35] For continuous films, the condition for crack extension does not depend on the crack length, but the film thickness.[35] With respect to crack formation, the patterned films of this study are more robust than continuous films, since the stored strain energy is lower due to relaxation during lateral shrinkage. However, as the line width becomes wider than a critical length, film cracking should again depend on the film thickness. The work of Beh *et al.*[19] illustrated that for ZrO_2 and SnO_2 films this limit is about 14 μm.

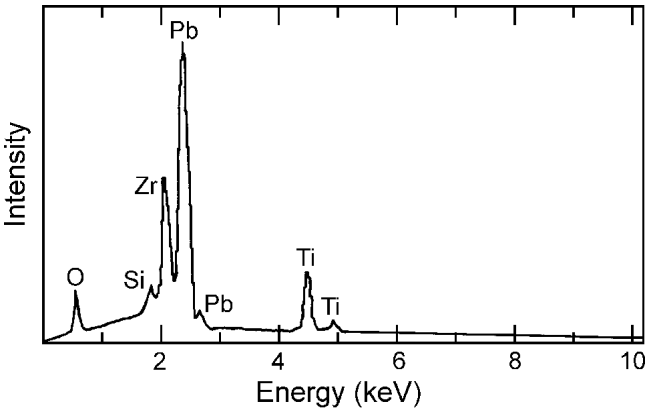

FIG. 9. EDS spectrum of micropatterned regions obtained from the sample shown in Fig. 2.

The patterned films on stainless steel plates displayed more lateral shrinkage than those on silicon and platinum coated silicon wafers. They also appeared to be weaker in the post-heat-treatment handling indicating weaker adhesion to the substrate. Thus, there seems to be a correlation between adhesive forces and the extent of lateral shrinkage of the patterned films.

IV. CONCLUSIONS

We demonstrated the utility of micromolding in capillaries method as a soft lithographic tool in the micropatterning of PZT films with line widths as small as 350 nm on Si, Pt/Si, and stainless steel. Defect-free areas as large as 1 cm^2 were fabricated with complex patterns. The robust processing of the films is attributed to the relaxation of stresses during drying and heat treatment through lateral shrinkage of the lines. In agreement with previous studies, the perovskite PZT phase nucleated and grew within a nanocrystalline fluorite (pyrochlore) matrix. Heat treatments at 600 °C yielded single-crystalline perovskite cross sections in micropatterned lines.

ACKNOWLEDGMENTS

We gratefully acknowledge the technical assistance of D.M. Dabbs and E.P. Luther. G.M. Whitesides and his group at Harvard University generously provided the patterned silicon wafers used in this work. This work was supported by an Army Research Office/Multidisciplinary University Research Initiative Program (Grant No. DAAH04-95-1-0102) and National Science Foundation (Grant No. INT98-10336). We also acknowledge partial support for MÖ from TÜBİTAK (Turkey), and from the NASA University Research Engineering and Technology Institute on Bio Inspired Materials (BIMat) under (Award No. NCC-1-02037).

REFERENCES

1. J.F. Scott and C.A. Paz de Araujo, Science **246,** 1400 (1989).
2. D.L. Polla, Microelect. Eng. **29,** 51 (1995).
3. D.L. Polla and L.F. Francis, Annu. Rev. Mater. Sci. **28,** 563 (1998).
4. L. O'Connor, Mech. Engin. **115,** 62 (1993).
5. P. Hauptmann, R. Lucklum, A. Püttmer, and B. Henning, Sens. Actuators A **67,** 32 (1998).
6. G. Rosenman, D. Shur, and A. Skliar, J. Appl. Phys. **79,** 7401 (1996).
7. W.B. Scott, Aviation Week Space Technol. **138,** 36 (1993).
8. D.F.L. Jenkins, M. Cunningham, and W.W. Clegg, Microelectr. Eng. **29,** 71 (1995).
9. P. Muralt, J. Micromech. Microeng. **10,** 136 (2000).
10. W.H. Ko, Sens. Actuators A **56,** 193 (1996).
11. N.L. Jeon, P.G. Clem, D.A. Payne, and R.G. Nuzzo, J. Mater. Res. **10,** 2996 (1995).
12. P.G. Clem, N-L. Jeon, R.G. Nuzzo, and D.A. Payne, J. Am. Ceram. Soc. **80,** 2821 (1997).
13. N-L. Jeon, P. Clem, D.Y. Jung, W. Lin, G.S. Girolami, D.A. Payne, and R.G. Nuzzo, Adv. Mater. **9,** 891 (1997).
14. M. Trau, N. Yao, E. Kim, Y. Xia, G.M. Whitesides, and I.A. Aksay, Nature **390,** 674 (1997).
15. P.D. Yang, T. Deng, D.Y. Zhao, D. Pine, B.F. Chmelka, G.M. Whitesides, and G.D. Stucky, Science **282,** 2244 (1998).
16. D.A. Payne and P.G. Clem, J. Electroceramics **3,** 163 (1999).
17. J.H. Kim, F.F. Lange, and C-I. Cheon, J. Mater. Res. **14,** 1194 (1999).
18. P.M. Moran and F.F. Lange, Appl. Phys. Letts. **74,** 9 (1999).
19. W.S. Beh, Y. Xia, and D. Qin, J. Mater. Res. **14,** 3995 (1999).
20. Y. Xia and G.M. Whitesides, Annu. Rev. Mater. Sci. **28,** 153 (1998).
21. A. Kumar and G.M. Whitesides, Appl. Phys. Lett. **63,** 2002 (1993).
22. A. Kumar, H.A. Biebuyck, and G.M. Whitesides, Langmuir **10,** 1498 (1994).
23. E. Kim, Y. Xia, and G.M. Whitesides, Nature **376,** 581 (1995).
24. Y. Xia, E. Kim, and G.M. Whitesides, Chem. Mater. **8,** 1558 (1996).
25. I.M. Reaney, K. Brooks, and R. Klissurska, J. Am. Ceram. Soc. **77,** 1209 (1994).
26. Y. Liu and P.P. Phule, J. Am. Ceram. Soc. **80,** 2410 (1997).
27. A.H. Carim, B.A. Tuttle, D.H. Doughty, and S.L. Martinez, J. Am. Ceram. Soc. **74,** 1455 (1991).
28. D.A. Barrow, T.E. Petroff, R.P. Tandon, and M. Sayer, J. Appl. Phys. **81,** 876 (1997).
29. G. Yi, Z. Wu, and M. Sayer, J Appl. Phys. **64,** 2717 (1988).
30. P. Guthner and K. Dransfeld, Appl. Phys. Lett. **61,** 1137 (1992).
31. B.A. Tuttle, T.J. Headley, B.C. Bunker, R.W. Schwartz, T.J. Zender, C.L. Hernandez, D.C. Goodnow, R.J. Tissot, J. Michael, and A.H. Carim, J. Mater. Res. **7,** 1876 (1992).
32. C.D.E. Lakeman, Z. Xu, and D.A. Payne, J. Mater. Res. **10,** 2042 (1995).
33. B.A. Tuttle, T.J. Headley, H.N. Al-Shareef, J.A. Voigt, M. Rodriguez, J. Michael, and W.L. Warren, J. Mater. Res. **11,** 2309 (1996).
34. F.F. Lange, Science **273,** 903 (1996).
35. J.W. Hutchinson and Z. Suo, in *Advances in Applied Mechanics*, edited by J.W. Hutchinson and T.Y. Wu (Academic Press, Boston, MA, 1992).